

## MIT Open Access Articles

*Pyrogallate#Based Metal#Organic Framework  
with a Two#Dimensional Secondary Building Unit*

The MIT Faculty has made this article openly available. **Please share**  
how this access benefits you. Your story matters.

**Citation:** Kampouri, Stavroula, Zhang, Mingxuan, Chen, Tianyang, Oppenheim, Julius J, Brown, Alexandra et al. 2022. "Pyrogallate#Based Metal#Organic Framework with a Two#Dimensional Secondary Building Unit." *Angewandte Chemie - International Edition*, 61 (49).

**As Published:** 10.1002/ANIE.202213960

**Publisher:** Wiley

**Persistent URL:** <https://hdl.handle.net/1721.1/148036>

**Version:** Final published version: final published article, as it appeared in a journal, conference proceedings, or other formally published context

**Terms of use:** Creative Commons Attribution-NonCommercial-NoDerivs License



## Metal-Organic Frameworks

How to cite: *Angew. Chem. Int. Ed.* **2022**, 61, e202213960

International Edition: doi.org/10.1002/anie.202213960

German Edition: doi.org/10.1002/ange.202213960

# Pyrogallate-Based Metal-Organic Framework with a Two-Dimensional Secondary Building Unit

Stavroula Kampouri, Mingxuan Zhang, Tianyang Chen, Julius J. Oppenheim, Alexandra C. Brown, Michael T. Payne, Justin L. Andrews, Junliang Sun, and Mircea Dincă\*

**Abstract:** We report a metal-organic framework (MOF) with a rare two-dimensional (2D) secondary building unit (SBU). The SBU comprises mixed-valent  $\text{Fe}^{2+}$  and  $\text{Fe}^{3+}$  metal ions bridged by oxygen atoms pertaining to the polytopic ligand 3,3',4,4',5,5'-hexahydroxybiphenyl, which also define the iron-oxide 2D layers. Overall, the anionic framework exhibits rare topology and evidences strong electronic communication between the mixed-valence iron sites. These results highlight the importance of dimensionality control of MOF SBUs for discovering new topologies in reticular chemistry, and especially for improving electronic communication within the MOF skeleton.

## Introduction

The rich compositional and structural diversity of metal-organic frameworks (MOFs) arises from permutations of their building units: the organic ligands and the secondary building units (SBUs).<sup>[1]</sup> However, it is not only the chemical composition that determines the properties of a given MOF; it is also essential to understand and control the arrangement of these chemical components in space – that is, the topology of the framework.<sup>[2]</sup> Indeed, topology plays a critical role in determining function, from gas separation and catalysis,<sup>[3]</sup> to electronic transport.<sup>[4]</sup>

Traditionally, topology in MOFs is controlled by changing the geometry and connectivity of the SBU and of the ligand.<sup>[5]</sup> It is less common to modify topology by changing the dimensionality of the SBU itself: the vast majority of

SBUs are zero-dimensional, or molecular.<sup>[6]</sup> Materials with one-dimensional SBUs, also known as rod-like SBUs, are also prominent and are often distinguished by the emergence of stronger electronic communication between the metal ions comprising the SBUs.<sup>[7]</sup> Following this logic, increasing the dimensionality should give rise to even more complex electronic structures and properties that mimic those of layered inorganic solids. However, further increasing the dimensionality of the SBU has proven difficult. In isolated examples, varying temperature and pH has been effective for modulating SBU dimensionality, but examples where the SBU dimensionality is determined or influenced by the functional group of the organic ligand are decidedly rarer.<sup>[8]</sup>

A promising strategy towards this end is the use of polytopic linkers bearing metal-binding atoms in close proximity, such as the pyrogallol moiety. Although underexplored in reticular chemistry, MOFs with pyrogallol-based linkers show promise in this sense, as they exhibit one-dimensional SBUs and display high stability.<sup>[9]</sup> An added potential attribute for pyrogallols is that they are redox-active and thus somewhat analogous to catechol-based ligands that have given rise to materials with strong electronic coupling.<sup>[10]</sup>

To explore the potential of pyrogallol ligands for forming high-dimensional SBUs, we targeted new MOFs derived from 3,3',4,4',5,5'-hexahydroxybiphenyl (HHBP, or di-pyrogallol). For the metal, we chose  $\text{Fe}^{2+}$  precursors, because iron-based MOFs containing infinite SBUs demonstrate stronger electronic interactions compared to their counterparts with other divalent ions, a property often ascribed to iron's propensity to form mixed-valent  $\text{Fe}^{2+/3+}$  phases.<sup>[10a]</sup>

## Results and Discussion

HHBP was prepared following a two-step synthetic protocol (Section S2.1, Supporting Information).<sup>[11]</sup> Solvothermal treatment of HHBP with four equivalents of  $\text{FeCl}_2$  in a mixture of *N,N*-dimethylformamide and water (volumetric ratio of 1:4) yielded  $\text{Fe}_3\text{HOBP}_{1.5}(\text{DMA})(\text{H}_2\text{O})_2$  ( $\text{FeHOBP}$ ,  $\text{HOBP} = 3,3',4,4',5,5'$ -hexahydroxybiphenyl) as a black crystalline powder (Section S2.2, Supporting Information). Attempts to improve crystallinity included the addition of modulators<sup>[12]</sup> such as triethylamine, pyrogallol, and nitric acid. Whereas triethylamine and pyrogallol led to amorphous solids, addition of up to 1.25 equivalents of nitric acid relative to

[\*] Dr. S. Kampouri, T. Chen, J. J. Oppenheim, A. C. Brown, M. T. Payne, Dr. J. L. Andrews, Prof. M. Dincă  
 Department of Chemistry, Massachusetts Institute of Technology  
 77 Massachusetts Avenue, Cambridge, MA 02139 (USA)  
 E-mail: mdinca@mit.edu

M. Zhang, Prof. J. Sun  
 College of Chemistry and Molecular Engineering, Beijing National Laboratory for Molecular Sciences, Peking University  
 Chengfu Rd, Haidian District, Beijing 100871 (China)

© 2022 The Authors. Angewandte Chemie International Edition published by Wiley-VCH GmbH. This is an open access article under the terms of the Creative Commons Attribution Non-Commercial NoDerivs License, which permits use and distribution in any medium, provided the original work is properly cited, the use is non-commercial and no modifications or adaptations are made.

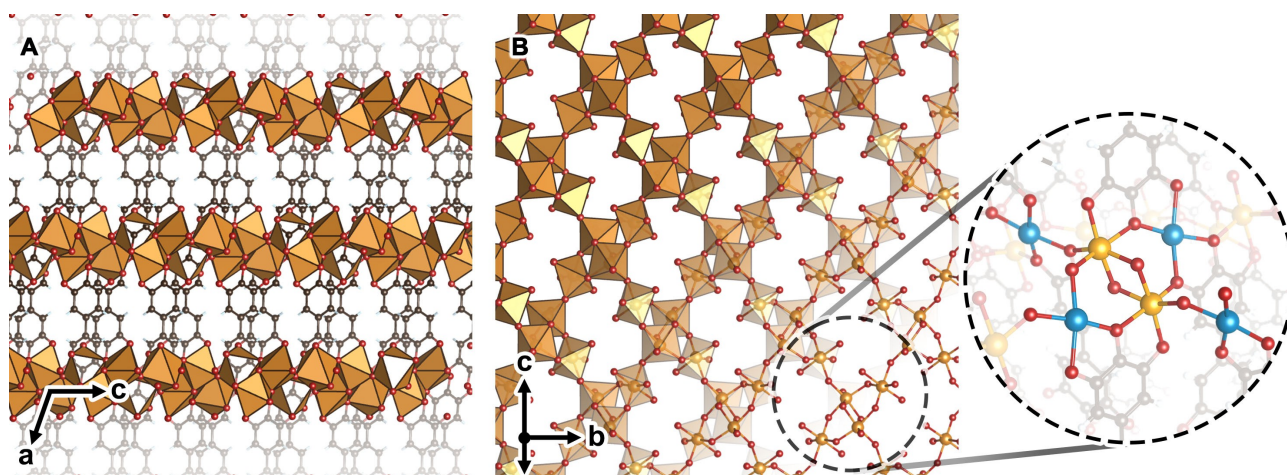


**Figure 1.** Structure of FeHOBP. View of the crystal structure along A) the  $(ac)$  plane, showing the connection of the 2D SBUs through the HOBP linkers, and B) along the  $(bc)$  plane, showing the 2D SBUs. Atoms corresponding to hydrogen and solvent molecules are omitted for clarity. The gray, red, and yellow spheres correspond to carbon, oxygen, and iron atoms, respectively.  $\text{FeO}_6$  octahedra are represented by solid orange polyhedra. In the selected area of the structure (B), the two crystallographically unique iron sites,  $\text{Fe}_{\text{sp}}$  and  $\text{Fe}_{\text{oct}}$  are represented by blue and yellow spheres, respectively.

HHBP led to slightly improved crystallinity, as determined by powder X-ray diffractometry (PXRD) (Figure S3, Supporting Information). This improvement in crystallinity by using an acid modulator is attributed to the increased reversibility of the linker-metal bond formation.<sup>[12]</sup>

Scanning electron microscopy (SEM) revealed that the as-synthesized material presents as thin plates, approximately  $4\ \mu\text{m}$  in width and  $10\ \mu\text{m}$  in length (Figure S4). Although the volume of these plates did not allow structural determination by single-crystal X-ray diffraction, the crystallites were sufficiently large for electron diffraction techniques (Section S5, Supporting Information). FeHOBP crystallizes in the monoclinic space group  $P2_1/c$  (Figure 1, see Table S2 for structural parameters).<sup>[13]</sup>

FeHOBP comprises an infinite two-dimensional (2D) SBU situated in the  $(bc)$  plane supported by pyrogallate moieties. Within the SBU there are two crystallographically independent, octahedral iron atoms. One ( $\text{Fe}_{\text{oct}}$ , oct: octahedral) is bound to four distinct HOBP ligands (two being  $\kappa_2$  and two being  $\kappa_1$ ), and the second ( $\text{Fe}_{\text{sp}}$ , sp: square planar) is bound to two distinct  $\kappa_2$  ligands, in addition to two axially-bound, heavily disordered solvent molecules (Figure 1B). Perpendicular to the SBU are one-dimensional channels that run parallel to the  $a$ -axis of the unit cell. The contents of these channels are heavily disordered, but likely contain charge-balancing dimethylammonium (DMA) cations that could not be resolved crystallographically (see below for molecular formula assignment).

The topology of the framework can be described using two different approaches. First, the application of a cluster simplification yields a 2D periodic **cpc** net, wherein one of the Fe atoms has three Fe nearest neighbors, and the other has four Fe neighbors (Figure 2).<sup>[14]</sup> This 2D net adopts an AAA-stacking configuration along the  $a$ -axis. A second topological analysis approach, employing the “standard simplification”—whereby each metal atom is considered as

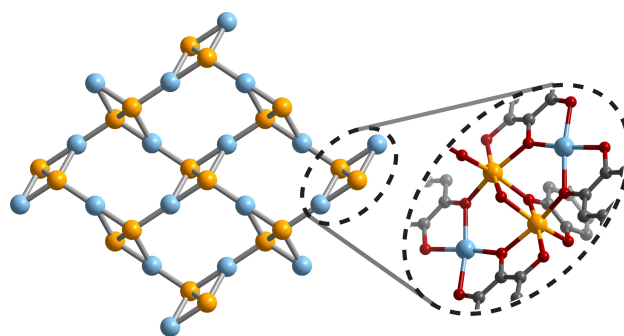


**Figure 2.** Schematic illustration of the FeHOBP topology through the cluster simplification approach, whereby the structure is broken down into parts with high connectivity. The two crystallographically independent iron sites,  $\text{Fe}_{\text{sp}}$  and  $\text{Fe}_{\text{oct}}$  are represented by blue and yellow spheres, respectively.

one node and the linkers as a separate node—yields a **4,6-c** net with 4,6T5 topology (Figure S11). To our knowledge, there is only one other example of such a net reported in the literature.<sup>[15]</sup>

The molecular formula of FeHOBP makes assumptions about the oxidation states of both the ligands and the Fe atoms, and is justified by a combination of structural analysis and spectroscopic investigations, as described below. Thus, the average aromatic C–C bond length in HOBP is  $1.390(8)\ \text{\AA}$ , consistent with a fully reduced pyrogallol.<sup>[16]</sup> The average C–O bond length is  $1.34(1)\ \text{\AA}$ , also close to that of pyrogallol,  $1.376(2)$ , and much longer than the C–O bond length observed in quinones,  $\approx 1.24\ \text{\AA}$ .<sup>[17]</sup> These bond lengths suggest that the most accurate depiction of the linker is in its fully reduced state,  $\text{HOBP}^{6-}$ .

Given the fully reduced state of the ligand, we surmised that the nearly black color of as-synthesized FeHOBP is the result of intervalence charge transfer, as would be expected for a mixed-valent Fe compound.<sup>[18]</sup> This was indeed verified

by Mössbauer spectroscopy (Section S8). More specifically, Mössbauer spectra collected at 80 K revealed peaks corresponding to  $\text{Fe}^{2+}$  and  $\text{Fe}^{3+}$  in a ratio of approximately 1:2 (Table S3). The Mössbauer doublets can be deconvoluted into three different  $\text{Fe}^{3+}$  sites and a unique  $\text{Fe}^{2+}$  site (Figure 3a). Each of the  $\text{Fe}^{3+}$  sites has an isomer shift of approximately  $0.55 \text{ mm s}^{-1}$  (consistent with high spin  $\text{Fe}^{3+}$  with  $S=5/2$ ) and quadrupole splitting of 0.394, 0.842, and  $1.302 \text{ mm s}^{-1}$ .<sup>[19]</sup> The  $\text{Fe}^{2+}$  center has an isomer shift of  $1.274 \text{ mm s}^{-1}$  and a quadrupole splitting of  $3.401 \text{ mm s}^{-1}$  (consistent with high spin  $\text{Fe}^{2+}$ ,  $S=2$ ). The four doublets can be interpreted as arising from the two unique crystallographic Fe sites. The presence of only one  $\text{Fe}^{2+}$  signal suggests that these iron sites occupy only one of the two crystallographically independent sites. Post-activation, the  $\text{Fe}^{3+}$  sites are indistinguishable from the as-synthesized sample; however, there are significant changes of the  $\text{Fe}^{2+}$  sites, resulting in the appearance of three unique features, with quadrupole splitting ranging from 2.618 to  $3.638 \text{ mm s}^{-1}$  (Figure S12). These results suggest that upon activation there are no changes to the apparent valency of the sites. Nevertheless, it appears that there is an increase in the heterogeneity of the coordination environment of the  $\text{Fe}^{2+}$  sites, which can be associated with solvent loss from this site. It is therefore reasonable to assign the  $\text{Fe}^{2+}$  centers as those that have bound solvent molecules.

Mixed valency in the  $\text{Fe}^{2+}/\text{Fe}^{3+}$  SBU was additionally confirmed by X-ray photoelectron spectroscopy (XPS, Section S9). The Fe 2p XPS spectrum of the MOF exhibits broad Fe  $2p_{3/2}$  and Fe  $2p_{1/2}$  peaks, which is typical for high spin  $\text{Fe}^{2+}/\text{Fe}^{3+}$  compounds.<sup>[20]</sup> Deconvolution of the Fe  $2p_{3/2}$  peak using the Gupta and Sen (GS) multiplets,<sup>[21]</sup> reveals the presence of both  $\text{Fe}^{2+}$  and  $\text{Fe}^{3+}$  species with a ratio of 1:2.2 (Figure 3b, Table S4), in line with the ratio observed by Mössbauer spectroscopy.

Electrochemical measurements confirmed that the HHBP linker can undergo reversible oxidation (Figure S17).

Although the possibility of mixed-valence ligands in the framework cannot be excluded, the absence of a carbonyl group stretching band in the IR spectrum strengthens the assignment of the ligand as a fully reduced  $\text{HOBP}^{6-}$ , on the basis of diffraction data and bond length analysis (Figure S10). Importantly, elemental analysis evinced the presence of nitrogen even after activation of the MOF (Table S5), suggesting the presence of a persistent, charge-balancing cation, likely dimethylammonium (DMA), a typical decomposition product during the thermolysis of DMF.<sup>[22]</sup> This is further supported by the XPS spectra of the activated MOF (Figure S16, Supporting Information), which exhibits a N 1s binding energy value at 400.3 eV, associated with alkyl ammonium.<sup>[23]</sup> These results combined with the absence of O–H stretching bands upon MOF activation—as demonstrated by IR spectroscopy (Figure S10)—confirm the assigned chemical formula of  $\text{Fe}_3\text{HOBP}_{1.5}(\text{DMA})(\text{H}_2\text{O})_2$  (FeHOBP) (vide supra).

$\text{N}_2$  adsorption data at 77 K revealed a Type II isotherm, typical for non-porous or macroporous materials. The limited  $\text{N}_2$  uptake can again be associated with DMA cations blocking the channels of FeHOBP that are otherwise visible from the crystallographic analysis (Figure S18). The thermal stability of FeHOBP was evaluated through means of thermogravimetric analysis, which showed a primary significant mass loss at  $\approx 165^\circ\text{C}$ , associated with the structural collapse of the framework (Figure S19). This decomposition temperature is similar to those of MOFs comprising pyrogallate-based linkers and has been associated with the oxidative decomposition of the phenolate moieties.<sup>[9a,c,d,f]</sup> The chemical stability of FeHOBP is notable and was confirmed by exposure to aqueous basic and acidic media. Thus, FeHOBP retains crystallinity after 16 hr in boiling water, in saline solution, as well as in buffer solutions with pH values of 4 and 10 (Figure S21). The chemical stability of FeHOBP can be associated both with the increased dimensionality of the SBU, and with the high  $\text{pK}_a$  value of

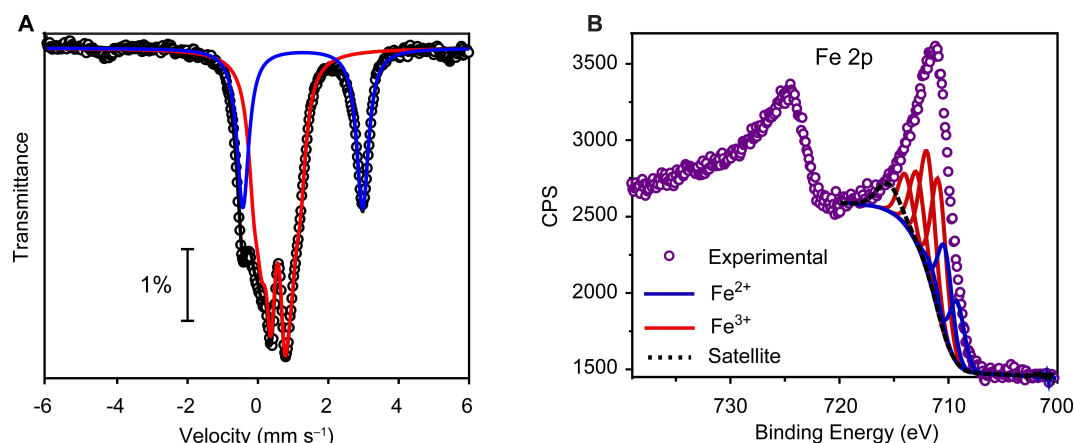


**Figure 3.** A) Mössbauer spectrum of activated FeHOBP, collected at 80 K. The black circles and solid black line correspond to the experimental data and their simulation, respectively. The simulation is according to the parameters in Table S3. The quadrupole doublet assigned to  $\text{Fe}^{2+}$  is shown in blue, and quadrupole doublets (3) assigned to  $\text{Fe}^{3+}$  are shown in red. B) High resolution XPS spectrum of the Fe 2p region. The binding energy of the first  $\text{Fe}^{3+}$  peak (710.4 eV) is typical for  $\text{Fe}^{3+}$  compounds with Fe–O coordination motifs, such as  $\text{FeOOH}$ . The binding energy of the first  $\text{Fe}^{2+}$  peak (708.8 eV) is typical for  $\text{Fe}^{2+}$  compounds with Fe–O coordination motifs, such as  $\text{FeO}$ . See Table S4 for fitting details.



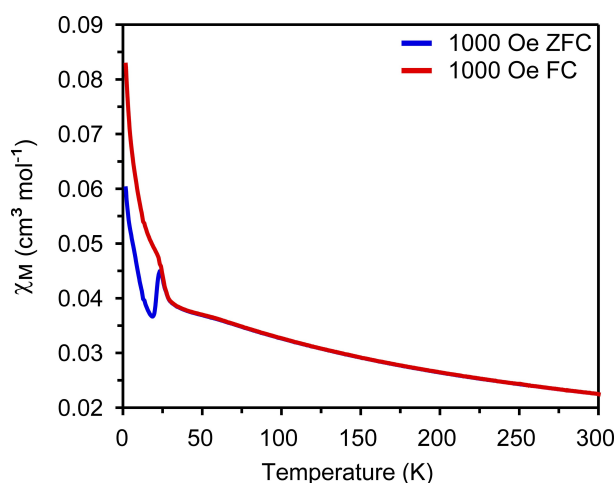


**Figure 4.** Variable-temperature zero-field-cooled (blue line) and field-cooled (red line) magnetic susceptibility for FeHOBP ( $H = 1.0$  kOe, DC).

pyrogallol,<sup>[24]</sup> resulting in strong metal-ligand interactions. These findings place FeHOBP among the chemically stable MOFs, a key feature for fully exploiting the potential of this class of materials.<sup>[25]</sup>

The diffuse reflectance was measured in the UV/Vis-NIR region, by diluting as-synthesized FeHOBP with potassium bromide ( $\approx 1$  wt. %). The Kubelka–Munk representation of the absorption spectrum reveals that FeHOBP manifests extended light absorption up to the NIR region (Figure S22a). The linear fit to the onset of absorption in Tauc coordinates reveals an optical band gap of 0.99 eV (Figure S22a, inset). The high energy absorption band at 250 nm can be associated with the HOBP ligand.<sup>[26]</sup> Although this feature appears blue-shifted compared to the UV/Vis absorbance of the free ligand (Figure S22b), it can be ascribed to stabilization upon its coordination to Fe in the framework. The features observed between 550–700 nm could be related to metal-ligand interactions and intervalence charge transfer (IVCT) between  $\text{Fe}^{2+}$  and  $\text{Fe}^{3+}$  centers, with the latter being observed previously with another Fe-based mixed-valence MOF.<sup>[27]</sup> The background absorption that tails in the NIR region is typically associated with increased free carrier concentrations.<sup>[28]</sup>

The extended light absorption of FeHOBP prompted us to probe its electrical conductivity, which was explored through both two-contact and four-contact probe methods, using pressed pellets of MOF powder.<sup>[29]</sup> The electrical conductivity of FeHOBP reaches  $10^{-6} \text{ Scm}^{-1}$  (Figures S23 and S24), situating it within the range of semiconducting MOFs, and highlighting the strong electronic coupling between the mixed-valent Fe sites within the 2D SBU. It should be noted that intrinsically, an oxygen-bridged mixed-valent  $\text{Fe}^{2+}/\text{Fe}^{3+}$  construct may not be expected to exceed the electrical conductivity of a natural mixed-valent oxide, such as  $\text{Fe}_3\text{O}_4$ , whose electrical conductivity indeed is  $10^{-6} \text{ Scm}^{-1}$  at room temperature.<sup>[30]</sup>

Magnetometry provided additional insight into the electronic communication between the Fe atoms in Fe-

HOBP (Section S17). Direct current (DC) magnetic susceptibility measurements of polycrystalline FeHOBP revealed complex exchange interactions that again resembled the susceptibility behavior of  $\text{Fe}_3\text{O}_4$  nanoparticles and non-stoichiometric perovskites.<sup>[31]</sup> The  $\chi_M T$  value for the formula  $\text{Fe}^{\text{III}}_2\text{Fe}^{\text{II}}(\text{HOBP})_{1.5}(\text{DMA})(\text{H}_2\text{O})_2$  at 300 K is  $6.71 \text{ cm}^3 \text{ K mol}^{-1}$ , which corresponds to  $7.33 \mu_B$ . This is significantly lower than the spin only value expected for the given formula ( $16.74 \mu_B$ ) and is in fact closest to the expected value for a single  $\text{Fe}^{2+}$  spin center ( $4.90 \mu_B$ ), suggesting that the  $\text{Fe}^{3+}$  spin centers have strong antiferromagnetic superexchange interactions even above room temperature. The  $\chi_M T$  value decreases to  $1.12 \text{ cm}^3 \text{ K mol}^{-1}$  at  $\approx 27$  K, further confirming the presence of strong antiferromagnetic coupling (Figure S27). This also agrees with the Curie–Weiss fitting of  $1/\chi_M T$  vs.  $T$  in the range of 200–300 K, which gives a Weiss temperature of  $-372$  K (Figure S28). The magnetic susceptibility  $\chi_M$  undergoes a sharp increase below  $\approx 27$  K, indicating a ferrimagnetic transition that likely arises from ferromagnetic double exchange interactions between  $\text{Fe}^{2+}$  and  $\text{Fe}^{3+}$  spin centers (Figure 4). Indeed, the divergence of zero-field cooling (ZFC) and field-cooling (FC) susceptibilities below  $\approx 27$  K further supports the arise of ferromagnetic interactions. Additional complexities, such as the cusp at  $\approx 23$  K in the temperature dependence of  $\chi_M$  indicates the appearance of additional antiferromagnetic coupling, possibly between  $\text{Fe}^{3+}$  spin centers that are more distant in the crystal structure. Similarly, the abrupt increase of  $\chi_M$  below 18 K suggests additional double exchange interactions between  $\text{Fe}^{2+}$  and  $\text{Fe}^{3+}$  spin centers. These results showcase that high dimensionality of the SBU allows for strong electronic coupling between the atoms comprising it, a deeper analysis of which will be treated in a future report.

## Conclusion

Examples of novel building units for the synthesis of MOFs are increasingly scarce. In this work, we found that the combination of the unexplored di-pyrogallol linker HHBP with iron precursors produces FeHOBP, a MOF with a unique topology that features a rare 2D SBU. The SBU comprises mixed-valent  $\text{Fe}^{2+}/\text{Fe}^{3+}$  sites, as evinced by Mössbauer spectroscopy and XPS. Electrical conductivity and magnetometry measurements reveal that the spatial configuration of the iron sites in the 2D SBU enables strong electronic interactions between them. Our findings highlight the advantage of designing MOFs encompassing high dimensional SBUs and can serve as a blueprint for the design of novel framework structures with properties distinctive to inorganic layered materials.

## Acknowledgements

This work was supported by the National Science Foundation (DMR-2105495). S. K. acknowledges financial support by the Swiss National Science Foundation, Grant P2ELP2\_195150. We would like to thank Dr. Harish Banda and Dr.

Ruperto G. Mariano for the electrochemical measurements, Dr. Yi Qu and Dr. Luming Yang for their help with magnetic measurements, and Dr. Davide Proserpio for discussions about the topological analysis.

### Conflict of Interest

The authors declare no conflict of interest.

### Data Availability Statement

The data that support the findings of this study are available in the supplementary material of this article.

**Keywords:** Coordination Polymers · MOFs · Mixed-Valency · Two-Dimensional SBUs

- [1] O. M. Yaghi, M. O'Keeffe, N. W. Ockwig, H. K. Chae, M. Eddaoudi, J. Kim, *Nature* **2003**, 423, 705–714.
- [2] A. Schoedel, *Metal-Organic Frameworks for Biomedical Applications*, Woodhead Publishing, London, **2020**, pp. 11–44.
- [3] H. Jiang, D. Alezi, M. Eddaoudi, *Nat. Rev. Mater.* **2021**, 6, 466–487.
- [4] C. Li, L. Zhang, J. Chen, X. Li, J. Sun, J. Zhu, X. Wang, Y. Fu, *Nanoscale* **2021**, 13, 485–509.
- [5] M. J. Kalmutzki, N. Hanikel, O. M. Yaghi, *Sci. Adv.* **2018**, 4, eaat9180.
- [6] a) F. M. Amombo Noa, M. Abrahamsson, E. Ahlberg, O. Cheung, C. R. Göb, C. J. McKenzie, L. Öhrström, *Chem* **2021**, 7, 2491–2512; b) J. Ha, J. H. Lee, H. R. Moon, *Inorg. Chem. Front.* **2020**, 7, 12–27.
- [7] N. L. Rosi, J. Kim, M. Eddaoudi, B. Chen, M. O'Keeffe, O. M. Yaghi, *J. Am. Chem. Soc.* **2005**, 127, 1504–1518.
- [8] A. K. Cheetham, C. N. R. Rao, R. K. Feller, *Chem. Commun.* **2006**, 4780–4795.
- [9] a) R. K. Feller, A. K. Cheetham, *Solid State Sci.* **2006**, 8, 1121–1125; b) E.-X. Chen, G. Xu, Q. Lin, *Inorg. Chem.* **2019**, 58, 3569–3573; c) G. Mouchaham, B. Abeykoon, M. Giménez-Marqués, S. Navalón, A. Santiago-Portillo, M. Affram, N. Guillou, C. Martineau, H. Garcia, A. Fateeva, T. Devic, *Chem. Commun.* **2017**, 53, 7661–7664; d) L. Cooper, N. Guillou, C. Martineau, E. Elkaim, F. Taulelle, C. Serre, T. Devic, *Eur. J. Inorg. Chem.* **2014**, 6281–6289; e) Z. Bao, J. Wang, Z. Zhang, H. Xing, Q. Yang, Y. Yang, H. Wu, R. Krishna, W. Zhou, B. Chen, Q. Ren, *Angew. Chem. Int. Ed.* **2018**, 57, 16020–16025; *Angew. Chem.* **2018**, 130, 16252–16257; f) L. Cooper, T. Hidalgo, M. Gorman, T. Lozano-Fernández, R. Simón-Vázquez, C. Olivier, N. Guillou, C. Serre, C. Martineau, F. Taulelle, D. Damasceno-Borges, G. Maurin, Á. González-Fernández, P. Horcajada, T. Devic, *Chem. Commun.* **2015**, 51, 5848–5851; g) E.-X. Chen, M. Qiu, Y.-F. Zhang, Y.-S. Zhu, L.-Y. Liu, Y.-Y. Sun, X. Bu, J. Zhang, Q. Lin, *Adv. Mater.* **2018**, 30, 1704388.
- [10] a) L. S. Xie, G. Skorupskii, M. Dincă, *Chem. Rev.* **2020**, 120, 8536–8580; b) R. Gusmão, V. López-Puente, I. Pastoriza-Santos, J. Pérez-Juste, M. F. Proença, F. Bento, D. Geraldo, M. C. Paiva, E. González-Romero, *RSC Adv.* **2015**, 5, 5024–5031.
- [11] S. J. Mills, C. Silvander, G. Cozier, L. Trésaugues, P. Nordlund, B. V. L. Potter, *Biochemistry* **2016**, 55, 1384–1397.
- [12] C. R. Marshall, E. E. Timmel, S. A. Staudhammer, C. K. Brozek, *Chem. Sci.* **2020**, 11, 11539–11547.
- [13] Deposition Number 2209895 contains the supplementary crystallographic data for this paper. These data are provided free of charge by the joint Cambridge Crystallographic Data Centre and Fachinformationszentrum Karlsruhe Access Structures service.
- [14] V. A. Blatov, A. P. Shevchenko, D. M. Proserpio, *Cryst. Growth Des.* **2014**, 14, 3576–3586.
- [15] L. Carlucci, G. Ciani, D. M. Proserpio, S. Rizzato, *CrystEngComm* **2003**, 5, 190–199.
- [16] a) R. Thakuria, S. Cherukuvada, A. Nangia, *Cryst. Growth Des.* **2012**, 12, 3944–3953; b) P. Pykkö, M. Atsumi, *Chem. Eur. J.* **2009**, 15, 12770–12779.
- [17] a) B. Kim, G. Storch, G. Banerjee, B. Q. Mercado, J. Castillo-Lora, G. W. Brudvig, J. M. Mayer, S. J. Miller, *J. Am. Chem. Soc.* **2017**, 139, 15239–15244; b) S. Roy, B. Sarkar, D. Bubrin, M. Niemeyer, S. Zális, G. K. Lahiri, W. Kaim, *J. Am. Chem. Soc.* **2008**, 130, 15230–15231.
- [18] M. B. Robin, P. Day, *Advances in Inorganic Chemistry and Radiochemistry, Vol. 10*, Academic Press, New York, **1968**, pp. 247–422.
- [19] B. Fultz, *Characterization of Materials, Mössbauer Spectrometry*, Wiley, Hoboken, **2012**, pp. 1–21.
- [20] A. Furlani, M. V. Russo, G. Polzonetti, K. Martin, H. H. Wang, J. R. Ferraro, *Appl. Spectrosc.* **1990**, 44, 331–334.
- [21] A. P. Grosvenor, B. A. Kobe, M. C. Biesinger, N. S. McIntyre, *Surf. Interface Anal.* **2004**, 36, 1564–1574.
- [22] a) H. He, L. Hashemi, M.-L. Hu, A. Morsali, *Coord. Chem. Rev.* **2018**, 376, 319–347; b) R. Seetharaj, P. V. Vandana, P. Arya, S. Mathew, *Arab. J. Chem.* **2019**, 12, 295–315.
- [23] *NIST Standard Reference Database*, **2000**, 20899.
- [24] B. Badhani, R. Kakkur, *Struct. Chem.* **2018**, 29, 359–373.
- [25] a) C. Wang, X. Liu, N. Keser Demir, J. P. Chen, K. Li, *Chem. Soc. Rev.* **2016**, 45, 5107–5134; b) N. C. Burtch, H. Jasuja, K. S. Walton, *Chem. Rev.* **2014**, 114, 10575–10612.
- [26] S. Selvaraj, P. Rajkumar, K. Thirunavukkarasu, S. Gunasekaran, S. Kumaresan, *Vib. Spectrosc.* **2018**, 95, 16–22.
- [27] L. S. Xie, L. Sun, R. Wan, S. S. Park, J. A. DeGayner, C. H. Hendon, M. Dincă, *J. Am. Chem. Soc.* **2018**, 140, 7411–7414.
- [28] D. A. Popescu, J.-M. Herrmann, A. Ensuque, F. Bozon-Verduraz, *Phys. Chem. Chem. Phys.* **2001**, 3, 2522–2530.
- [29] L. Sun, S. S. Park, D. Sheberla, M. Dincă, *J. Am. Chem. Soc.* **2016**, 138, 14772–14782.
- [30] A. Radoń, D. Łukowiec, M. Kremzer, J. Mikuła, P. Włodarczyk, *Materials* **2018**, 11, 735.
- [31] a) M. Suzuki, S. I. Fullem, I. S. Suzuki, L. Wang, C.-J. Zhong, *Phys. Rev. B* **2009**, 79, 024418; b) H. L. Feng, M. Reehuis, P. Adler, Z. Hu, M. Nicklas, A. Hoser, S.-C. Weng, C. Felser, M. Jansen, *Phys. Rev. B* **2018**, 97, 184407.

Manuscript received: September 21, 2022

Accepted manuscript online: September 30, 2022

Version of record online: November 7, 2022